agriculture

MDPI

Article

SENSE-GDD: A Satellite-Derived Temperature Monitoring Service to Provide Growing Degree Days

Iphigenia Keramitsoglou [1,*], Panagiotis Sismanidis [1,2], Olga Sykioti [1], Vassilios Pisinaras [3], Ioannis Tsakmakis [3], Andreas Panagopoulos [3], Argyrios Argyriou [4] and Chris T. Kiranoudis [1,5]

[1] Institute for Astronomy Astrophysics Space Applications and Remote Sensing, National Observatory of Athens, Vas. Pavlou & I. Metaxa, 15236 Penteli, Greece; panosis@noa.gr (P.S.); sykioti@noa.gr (O.S.); kyr@chemeng.ntua.gr (C.T.K.)
[2] Institute of Geography, Ruhr University Bochum, 44801 Bochum, Germany
[3] Soil and Water Resources Institute, Hellenic Agricultural Organization—DEMETER, 57400 Sindos, Greece; v.pisinaras@swri.gr (V.P.); i.tsakmakis@swri.gr (I.T.); a.panagopoulos@swri.gr (A.P.)
[4] Gerovassiliou Estate, 57500 Epanomi, Greece; viticulture@gerovassiliou.gr
[5] School of Chemical Engineering, National Technical University of Athens, 15773 Athens, Greece
* Correspondence: ik@noa.gr; Tel.: +30-210-34090867

Abstract: A new satellite-enabled interoperable service has been developed to provide high spatio-temporal and continuous time series of Growing Degree Days (GDDs) at the field. The GDDs are calculated from MSG-SEVIRI data acquired by the EUMETCast station operated by IAASARS/NOA and downscaled on-the-fly to increase the initial coarse spatial resolution from the original 4–5 km to 1 km. The performance of the new service SENSE-GDD, in deriving reliable GDD timeseries at dates very close to key phenological stages, is assessed using in situ air temperature measurements from weather stations installed in Gerovassiliou Estate vineyard at Epanomi (Northern Greece) and an apple orchard at Agia (Central Greece). Budburst, pollination, and the start of veraison are selected as key phenological stages for the vineyards, whilst budburst and pollination for the apple orchard. The assessment shows that SENSE-GDD provided uninterrupted accurate measurements in both crop types. A distinct feature is that the proposed service can support decisions in non-instrumented crop fields in a cost-effective way, paving the way for its extended operational use in agriculture.

Keywords: growing degree days; temperature; satellite; earth observation; MSG-SEVIRI; agriculture

Citation: Keramitsoglou, I.; Sismanidis, P.; Sykioti, O.; Pisinaras, V.; Tsakmakis, I.; Panagopoulos, A.; Argyriou, A.; Kiranoudis, C.T. SENSE-GDD: A Satellite-Derived Temperature Monitoring Service to Provide Growing Degree Days. *Agriculture* **2023**, *13*, 1108. https://doi.org/10.3390/agriculture13051108

Academic Editor: Weiwei Chen

Received: 25 April 2023
Revised: 16 May 2023
Accepted: 17 May 2023
Published: 22 May 2023

1. Introduction

Heat units, expressed in the form of growing degree days (GDDs), have been extensively used in agricultural research to monitor crop development and to assess potential differences in crop growth patterns [1]; changes in crop diurnal development rates [2]; and potential response of crop growth rates under short- and long-term future climate change scenarios [3–5]. Moreover, directly (as an indicator that signifies the beginning/ending of critical phenological stages/periods [6]) or indirectly (e.g., as an input to crop models [7,8]), GDDs are increasingly used to optimize the overall farming decision making, from variety selection to enhancing field management practices, such as irrigation and weed control. Specifically, in the case of irrigation, GDD accumulation can guide irrigation, e.g., from full irrigation to mild regulated deficit irrigation [9,10], while for weed control, a certain accumulation of GDDs triggers the beginning and the end of critical weed-control periods [11,12]. This is the reason why GDD is often incorporated into irrigation models, such as the AquaCrop model [13–15], proposed variations of AquaCrop [16], and other models [17].

The calculation of GDDs is commonly based on in situ instrumentation, e.g., weather stations measuring air temperature (AT) [18–21]. However, in several cases, the high equipment costs, as well as the annual costs related to data transmission and storage ren-

der the acquisition and maintenance of such equipment prohibitive (especially in small-scale farming). As an alternative, methods that calculate GDDs remotely via satellite data have been very recently reported in the literature [22–24]. For example, [22] use satellite-derived evapotranspiration estimates, land surface temperature (LST) measurements, and crop phenological stage information for Nebraska maize crops to quantify how irrigation covers water and temperature stresses. The calculation of the GDD and Extreme Degree Days (EDD) is conducted using daily 1 km LST data from the MYD11A1 data product, interpolated to hourly values using a sine function to characterize the maize crop surface temperatures during the period 2003–2016 [22]. The measurements are compared to daily minimum and maximum surface AT at 1 km resolution from Daymet version 3 [25] providing high to moderate accuracies. Moreover, [23,24] use temperature measurements retrieved from the Climate Date Store (CDS) of Copernicus Climate Change (C3S) Service [26], which provides information about the past, present, and future climate, on the global, continental, and regional scale from a variety of data sources, including satellite observations [26]. In particular, [23] exploit satellite-derived data to provide weekly global water-demand index maps for the period 2016–2020 based on a parameter-independent data-driven approach using available remote sensing products and weather data, such as soil moisture, normalized difference vegetation index (NDVI), and GDD measurements. In particular, the GDD data are calculated using hourly AT estimates at 2 m above ground retrieved from CDS with temporal and spatial resolutions of 1 h and 0.1° × 0.1° (approx. 10 km), respectively. On the other hand, [24] test three models for a continuous in-season and/or post-season wheat yield assessments of wheat crops in Central Greece by fully exploring the Copernicus CDS data sets. In particular, GDD is calculated using gridded agrometeorological data for the 2019–2021 growing seasons at a spatial resolution of 0.1° × 0.1° and of 0.25° × 0.25° (approx. 25 km) derived from the ERA5-Land and ERA5 re-analysis, respectively, that are generated by the European Centre for Medium-Range Weather Forecasts (ECMWF) and freely distributed through CDS. Measurements include hourly data consisting of 2 m air temperature, aggregated into daily means and/or sums.

The Agricultural Interoperability and Analysis System (ATLAS) is a European H2020 funded project, the goal of which is to develop an open interoperability network for agricultural applications and to build a sustainable ecosystem for innovative data-driven agriculture (https://www.atlas-h2020.eu/; accessed on 24 April 2023). ATLAS network is based on a service-oriented architecture which offers a high level of scalability from a single farm to a global community. The technology developed in ATLAS is tested and evaluated within pilot studies on a multitude of real agricultural operations across Europe. ATLAS involves all actors along the food chain, simplifying and improving the processes from farm to fork. Through the support of innovative start-ups, small and medium-sized enterprises (SMEs), and farmers, ATLAS enables new business models for the farmers and establishes sustainable business ecosystems based on innovative data-driven services. In parallel, the establishment of a Representational State Transfer (REST) architecture as the best standard to design and deploy internet of things applications (IoT apps) in server-cloud environments [27,28], in combination with secure transfer protocols, such as OAuth 2 (Open Authorization) [29], has rendered the interconnection and interoperability between IoT apps fast, reliable, and secure.

Within the framework of its partnership with the ATLAS project, the Institute for Astronomy, Astrophysics, Space Applications and Remote Sensing (IAASARS) of the National Observatory of Athens (NOA) developed and implemented an innovative, real-time, operational, interoperable temperature monitoring service that provides cumulative GDD time series for a given time and location, derived from satellite data. The present work overcomes the two main drawbacks of thermal infrared imagery, namely coarse spatial resolution and cloud coverage.

In this paper, we present (a) the service methodology and communication schema within the ATLAS ecosystem; and (b) a service performance evaluation based on data collected from in situ weather stations installed in two different locations and crop types in Greece.

2. Materials and Methods

2.1. Data

2.1.1. Data Necessary for the Satellite Retrievals

Satellite-derived services are developed using high spatiotemporal land surface and AT datasets that are combined with crop-specific characteristics to calculate the GDD. Four different types of datasets are used:

1. Satellite Radiance at Top-of-Atmosphere data series acquired from the Meteosat Second Generation Spinning Enhanced Visible and InfraRed Imager (MSG SEVIRI) instrument: SEVIRI is a 50 cm diameter aperture, line-by-line scanning radiometer, which provides image data in four Visible and Near-InfraRed (VNIR) channels and eight thermal InfraRed (TIR) channels. A key feature of SEVIRI is its continuous imaging of the Earth with a baseline repeat cycle of 15 min. The VNIR spectral range is 0.4–1.6 μm and the TIR is 3.9–13.4 μm [30]. The TIR channels provide, among other information, continuous data about the temperatures of clouds, land, and sea surfaces. For the purposes of this work, the data from TIR channels are used. Due to the full disk viewing geometry, the spatial resolution of SEVIRI data varies with geographic latitude and over Europe it ranges from approximately 4 km at 35° to 6 km at 50° N.
2. Elevation data from the Shuttle Radar Topography Mission (SRTM) global Digital Elevation Model (DEM): The elevation data are provided as 1° × 1° tiles with a spatial resolution of 30 m. Here, we use all the tiles that cover Europe and we resample them to 1 km using spatial averaging [31].
3. Numerical Weather Predictions: Atmospheric profiles of temperature and relative humidity are retrieved from the Global Forecasting System (GFS) and interpolated to hourly values [32].
4. Base temperature per crop: As temperature increases above the base temperature, plants develop progressively. This information is provided by the crop specialists.

2.1.2. Validation Data

The capability of the service to derive reliable GDD timeseries and thus support decisions that depend on key phenological stages is assessed using temperature measurements from weather stations installed in the designated agricultural pilot areas of ATLAS. These pilot areas include vineyards located in a flat, coastal plain area at Epanomi (Northern Greece; 40.450645° N; 22.920283° E; elev.: 80 m a.s.l.) and an apple orchard located at Agia (Central Greece; 39.719385° N; 22.739093° E; elev.: 204 m a.s.l.), both shown in Figure 1. The vineyards at Epanomi are cultivated with the white grape variety Malagouzia and the red grape variety at Limnio, while the apple orchard of Agia with the Granny Smith variety. Both stations measure AT every 15 min, and then transmit the measurements, almost in real-time, to cloud data storage. In the case of vineyards, the station was installed in March 2021, while in the apple orchard it was installed in February 2022. For the purposes of this study, the AT measurements of 2021 and 2022 are retrieved and used for the vineyards and measurements of 2022 are used for the apple orchard.

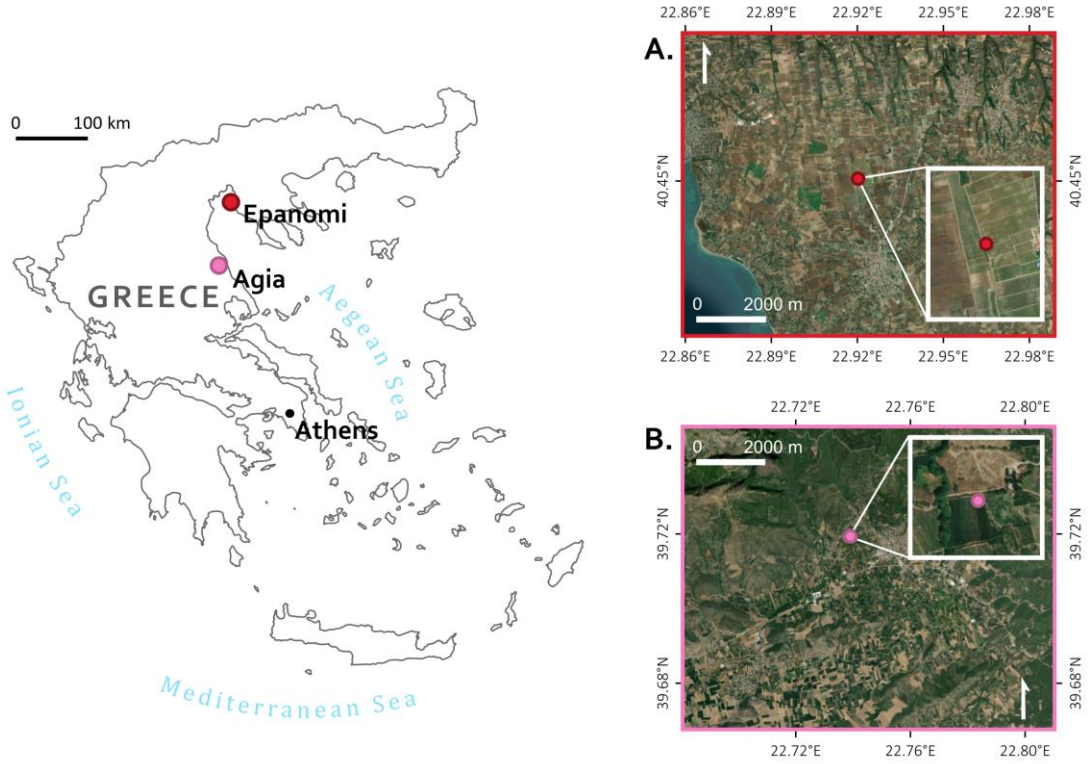

Figure 1. ATLAS agricultural pilot areas used as case studies for evaluating SENSE-GDD: (**A**) Epanomi (vineyard with two grape varieties) and (**B**) Agia (apple orchard).

2.2. Methodology

The methodology for the calculation of the SENSE-GDD product and its integration in the ATLAS Ecosystem Interoperability Architecture is presented below.

2.2.1. Satellite-Derived GDD Calculation

AT data are retrieved from the satellite-based nowcasting service of IAASARS/NOA [33]. This service has been designed originally to monitor the urban environment [34–37] and is now customized for monitoring agricultural areas to support decisions relevant to irrigation needs and automated services. To achieve this purpose, four requirements have been identified:

1. production of continuous time series of AT data with increased spatial and temporal resolution (1 km/1 h),
2. operation in real time and online,
3. ability to cover any part in Europe, and
4. elimination of down-time and data gaps, as GDD is a cumulative measure of AT and days with missing data can cause significant deviations.

To fulfil these requirements, a composite workflow was devised that relies on the combined exploitation of thermal remote sensing data from MSG-SEVIRI and an advanced spatial enhancement algorithm [33,34]. Geostationary satellite image data are a prominent data source, because (i) they cover a large area of the Earth; (ii) they are acquired with high frequency (1 image every 5 min); (iii) they can be retrieved in real time through data acquisition antennas, instead of downloading from the satellite service providers; and (iv) they can be downscaled to finer spatial resolutions (1 km or even finer). The GDD calculation is performed in the following two stages.

- Stage 1: Retrieval of AT data from satellite thermal images

The process of retrieving the AT from the MSG-SEVIRI image data involves several steps. The first step is the real-time image acquisition and preprocessing. Next, a cloud

mask (CMa) is prepared by delineating all the areas covered by clouds. Then, the image segments that correspond to the ATLAS pilot sites are clipped and the land surface temperature and AT of each pixel are retrieved using the data assimilation method proposed in [33]. Finally, the temperature data are downscaled to 1 km using statistical downscaling [33]. The downscaling algorithm is based on a support vector machine (SVM) coupled with gradient boosting and uses as predictors elevation data, vegetation indices, and information about the LST annual climatology. The downscaling is performed on-the-fly and a new SVM model is created for each hourly AT image, as explained in [33,36]. To generate the spatially enhanced AT data, we train each SVM model to predict the hourly AT from the coarse-scale predictors (resampled to the coarse-scale SEVIRI grid) and then apply it to the original 1 km predictors. These five operations run sequentially each time the satellite transmits a new image to the ground.

- Stage 2: Calculation of GDD

Considering that GDD is used to estimate the growth and development of plants and weeds during the growing season, the basic concept is that development will only occur if the average daily temperature (Equation (1)) exceeds a certain air temperature threshold; called the base temperature (T_{base}). T_{base} may vary significantly between crops and varieties. If the daily mean AT (T_{ave}) is equal or below T_{base}, then the GDD value is zero, indicating that even though calendar time passed, plant development did not progress accordingly (Equation (2)). If T_{ave} is above T_{base}, then the GDD equals the difference between T_{ave} and T_{base} [38].

$$T_{\text{ave}} = \frac{T_{\max} - T_{\min}}{2} \tag{1}$$

$$\text{GDD} = \begin{cases} T_{\text{ave}} - T_{\text{base}} & \text{if } T_{\text{ave}} > T_{\text{base}} \\ 0 & \text{if } T_{\text{ave}} \leq T_{\text{base}} \end{cases} \tag{2}$$

Subsequently, the cumulative GDD (GDDs) over a target period (e.g., from budburst to flowering) were calculated according to Equation (3):

$$\text{GDDs} = \sum_{i=1}^{n} \text{GDD}_i \tag{3}$$

where, i is the calendar date. Despite the name, Growing Degree Days are cumulative temperature differences and are therefore expressed in temperature units. Often in practice, the units are omitted.

2.2.2. ATLAS Ecosystem Interoperability Architecture

The structural components of the ATLAS ecosystem are the individual services, which are grouped according to their functionality. For instance, all services that potentially provide temperature data and related parameters (such as SENSE-GDD) are placed under the "temperature monitoring" services. An individual service communicates and exchanges data with the other services via RESTful API architecture, as demonstrated in the following example. Say that a farmer uses the ATLAS ecosystem to get the GDDs for his/her farm. The first step is to register his/her farm in ATLAS's "field data" service. For the SENSE-GDD to be able to access the farm, the two services must be "paired". Pairing is a procedure that retrieves assets from both services (in this example the "field data" and "temperature monitoring" services) and stores them automatically in a database. The assets will be later used to obtain all necessary farm info by calling the backend of each service with the relevant authorization flow. This procedure is implemented using a web app. Pairing is accomplished after successful service logins. Likewise, if the farmer wishes to acquire irrigation advice based on the GDD information, he/she must register for the relevant service. In this case, SENSE-GDD will get farm data from the "field data" service and provide data to the "irrigation advisor" service with similar authorization procedures.

The above-mentioned example presents just a fraction of the service pools that are hosted within the ATLAS ecosystem, as well as a simplified example of the potential interoperable communication paths (Figure 2). A detailed description of the system architecture, required authentication protocols during requests and analytical guidelines about how the services of each pool must implement their APIs can be found at https://github.com/atlasH2020-templates and https://github.com/atlasH2020 (both accessed on 24 April 2023).

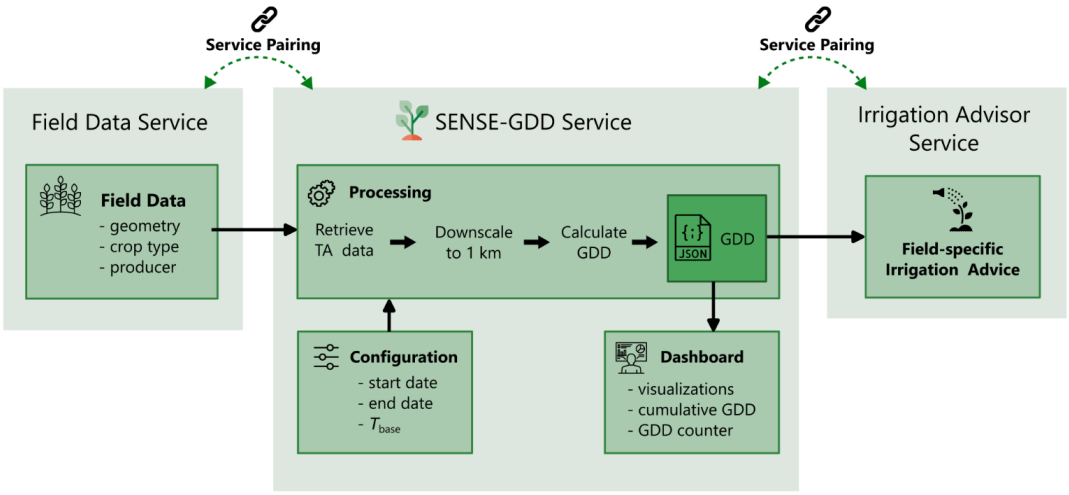

Figure 2. A simplified example of potential interoperable communication paths in the ATLAS ecosystem that use SENSE-GDD.

- SENSE-GDD basic functions within ATLAS ecosystem

The role of SENSE-GDD within the ATLAS ecosystem is to provide individual services with cumulative GDD timeseries for a given location and time period. In brief, the service accepts REST API POST method requests. The POST request body must be a JavaScript Object Notation (JSON) script with the following keys:

- *field_unique_ref_code*
- *base_temperature*
- *start_date*
- *end_date*

where, *"field_unique_ref_code"* is the field-ID in a string format; *"base_temperature"* an integer whose meaning is explained in detail in Section 2.2.1; and *"start_date"* and *"end _date"* the first and last date of requested time series, provided in ISO 8601 format, respectively.

The service then calculates the GDD on the fly and returns an array of JSON objects, whose number is equal to the number of days between *"start_date"* and *"end_date"*. For example, for *"start_date"* 1 April 2021 and *"end_date"* 31 May 2021, an array of 61 JSON objects will be prepared and returned. Each JSON object includes the keys *"gdds_cumulative"* and *"date"*, with the former representing the value cumulative GDDs and the latter the corresponding date.

2.3. Assessment of SENSE-GDD Product Performance

The SENSE-GDD's capability to derive accurate and precise GDD time-series is evaluated from two different perspectives. Initially, the daily GDD time-series that are derived from SENSE-GDD are compared with corresponding GDD data obtained from the in situ AT measurements. The difference between the two GDD time-series is quantified using the coefficient of determination (R^2); the Root Mean Square Difference (RMSD; Equation (4)) and the Mean Absolute Deviation (MAD; Equation (5)):

$$\mathrm{RMSD} = \sqrt{\frac{\sum_{i=1}^{n}\left(\mathrm{GDD}_{\mathrm{s},i} - \mathrm{GDD}_{\mathrm{r},i}\right)^2}{n}} \quad (4)$$

$$\mathrm{MAD} = \frac{1}{n}\sum_{i=1}^{n}\left|\mathrm{GDD}_{\mathrm{s},i} - \mathrm{GDD}_{\mathrm{r},i}\right| \quad (5)$$

where, n is the number of measurements, $\mathrm{GDD_s}$ is the daily GDD calculated by SENSE-GDD using Equation (2) and $\mathrm{GDD_r}$ is the reference in situ GDD.

For the Malagouzia and Limnio varieties, T_{base} is set equal to 10°C, based on consultation with the agronomist of Gerovassiliou Estate, and in agreement with the value proposed by the FAO Irrigation and Drainage Paper 66: Crop yield Response to Water for wine grapes [39]. The same base temperature (10°C) is selected for the apple orchard, according to previous reported experimental data [40].

The cumulative GDD and the date of key phenological stages of the three crop types are also used for assessing the performance of SENSE-GDD. Budburst, pollination, and the start of veraison are selected as key phenological stages for the two wine grape types in Epanomi (Malagouzia and Limnio) and budburst and pollination for the Granny Smith apple orchard in Agia. Observations in vineyards were performed in situ by the winery agronomists to determine the calendar date that each key stage started in the 2021 and 2022 cultivation periods. A network of field-installed cameras was used to monitor the apple trees canopy development in 2022 and the photos were used to determine the budburst and flowering stages. The analysis of the camera photos showed that the buds of the Granny Smith apple trees burst on 4 March 2022, while tree flowering phase began just 10 calendar days later, on 13th April. To assess the SENSE-GDD's capability to provide the phenological stages based on GDDs as closely as possible to a weather station, we first calculated the cumulative GDDs (Equation (3)) from the in situ data, using as start date the observed budburst date and as end date the flowering or veraison (only for vineyards) dates. Then, we compared the in situ cumulative GDD calculated for each phenological stage against the corresponding data retrieved from SENSE-GDD, in order to identify on which calendar date the SENSE-GDD and the in situ estimates are approximately equal:

$$\underset{i \in \mathcal{I}}{\mathrm{argmin}}\left\{\left|\mathrm{GDDs}_{\mathrm{s},i} - \mathrm{GDDs}_{\mathrm{r},i}\right|\right\} \quad (6)$$

In Equation (6), $\mathrm{GDDs}_{\mathrm{s},i}$ and $\mathrm{GDDs}_{\mathrm{r},i}$ are the cumulative GDD calculated from the SENSE-GDD and the in situ data (both using Equations (1)–(3)), respectively, i is the calendar date, and $\mathcal{I}$ the set of all calendar dates between the start and end date. Finally, to assess if the SENSE-GDD assessment drifts, we calculate the absolute and relative differences between the SENSE-GDD and in situ cumulative GDDs at the end date.

3. Results and Discussion

3.1. Sense-GDD Web Service

In addition to the REST API, a web service has also been developed for obtaining and visualizing the GDD from any device, as shown in Figure 3. To use the web service, the user must start by selecting his/her field from map panel ① and then set the start and end dates noted with ②. In the example of Figure 3, which focuses on the Malagouzia vineyard of Gerovassiliou Estate in 2021, the start date is set to the date of budburst (07 April 2021) and the end date is set to a date after veraison (31 July 2021), while the base temperature is set to 10°C (shown with ③ in Figure 3). To display the result, the user has to click the "GDDs" button noted with ④, and the GDD result will be presented by means of a cumulative plot (⑤ in Figure 3) and a counter showing the resultant GDD on the end date (⑥ in Figure 3).

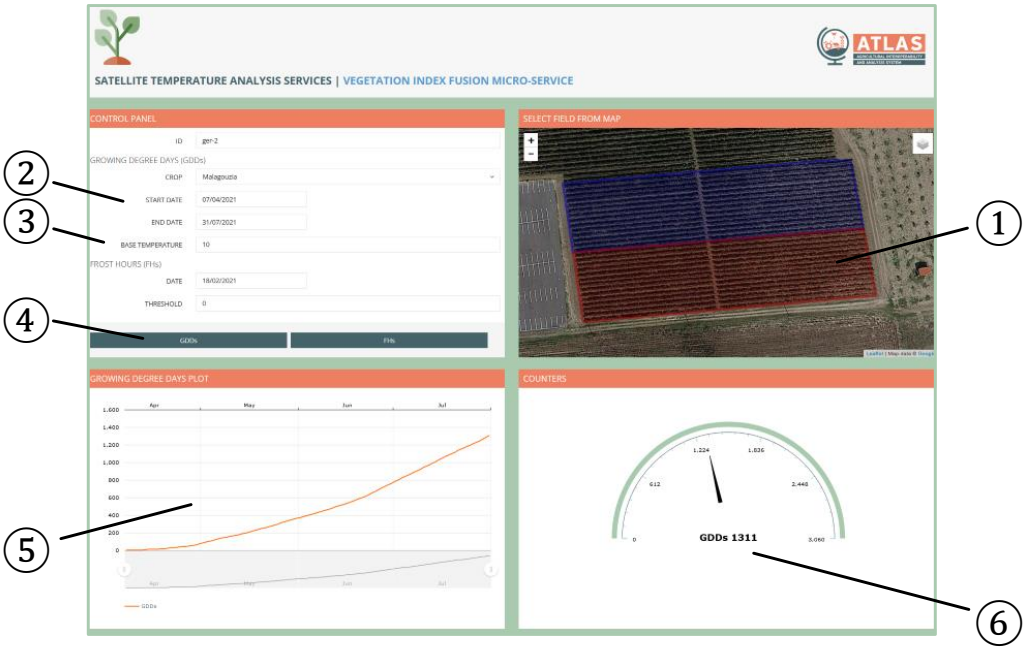

Figure 3. Example of the SENSE-GDD web service: ① the location of the crop shown on map; ② the start and end date provided by the user; ③ the base temperature for the specific crop; ④ the button for GDDs calculation; ⑤ the cumulative GDDs plot; (6) the counter view of the GDD for the end date.

3.2. Evaluation against in situ Daily GDD

For the three case studies and crop types, the daily GDD (calculated using Equation (2)) issued from SENSE-GDD are compared with the corresponding ones measured by the in situ weather stations (Figure 4).

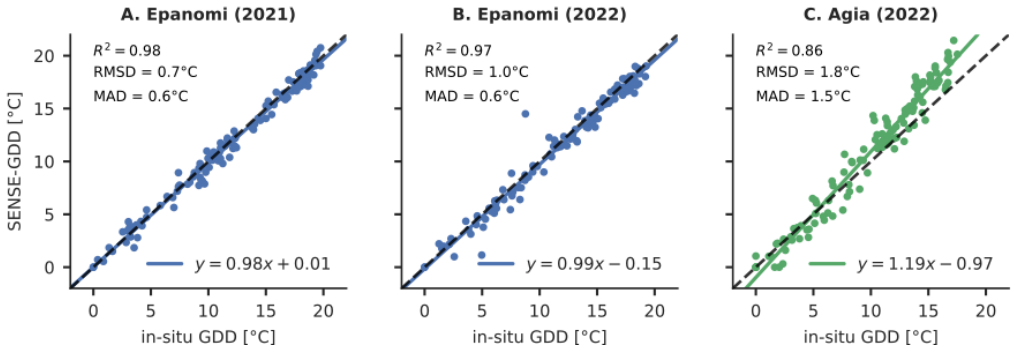

Figure 4. Scatterplots of daily GDD calculated from SENSE-GDD versus in situ daily GDD and corresponding linear fit equations and performances for Gerovassiliou Estate vineyard at Epanomi spanning (**A**) April–July 2021 and (**B**) April–July 2022; and (**C**) apple orchard at Agia spanning mid-June to July 2022.

The daily GDD calculated by the satellite-enabled service SENSE-GDD and the in situ measurements show a strong agreement for both crop types with a $R^2 \geq 0.86$ (Figure 4). The highest agreement is observed for Epanomi site in 2021 ($R^2 = 0.98$) and the lowest for the Granny Smith apples at Agia ($R^2 = 0.86$). The RMSD for all crop types is low. For Epanomi (Figure 4A,B), the lowest value is observed for 2021 (0.7°C) and it increases slightly in 2022 (1.0°C). The RMSD for the Agia site is higher (1.8°C) than that of Epanomi (as does MAD), something we attribute to the more pronounced topography of the Agia region. Generally, the results for 2021 are slightly better than that for 2022, but in both cases the performance of SENSE-GDD is considered highly adequate for any operational use.

3.3. Cumulative GDD and Crop Phenological Stages

The comparison between the cumulative GDD derived from SENSE-GDD and the in situ data for the three crop types with the corresponding phenological stages is presented in Figure 5. The dates of each key phonological stage for each crop type are presented in Table 1. Concerning cumulative GDD, the two GDD curves, namely the one generated from SENSE-GDD data and the one from in situ measurements, coincide at the beginning of the growing seasons for all cases. Due to the nature of cumulative variables, the differences between the satellite-enabled and in situ GDD slightly increase with time as any discrepancy is added up.

Table 1. Dates of the key phenological stages for the grape vine varieties and apples issued from in situ measurements and SENSE-GDD. Calendar days of budburst, pollination and veraison stages are observed in Malagouzia and Limnio vineyards during 2021 and 2022 cultivation seasons. For the Granny Smith apple orchard budburst and pollination stages are observed for 2022.

Crop	Phenological Stage	Date in 2021		Date in 2022	
		In situ	SENSE-GDD	In situ	SENSE-GDD
Limnio	Budburst	09/04	09/04	07/04	07/04
	Pollination	26/05	26/05	24/05	26/05
	Veraison	22/07	24/07	20/07	22/07
Malagouzia	Budburst	07/04	07/04	05/04	05/04
	Pollination	21/05	21/05	19/05	21/05
	Veraison	18/07	19/07	16/07	18/07
Granny Smith Apples	Budburst	-	-	03/04	03/04
	Pollination	-	-	13/04	15/04

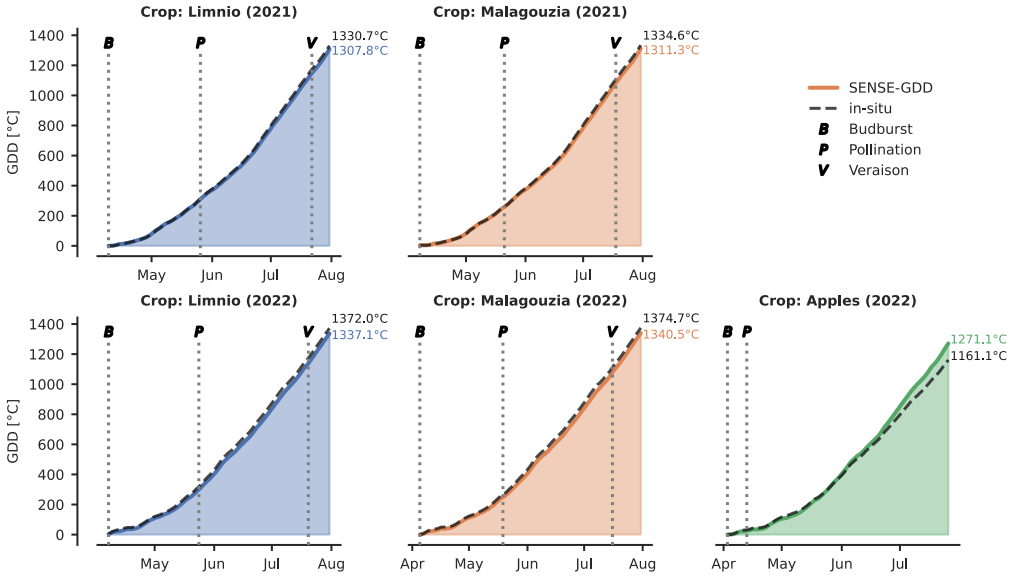

Figure 5. Cumulative GDD derived from SENSE-GDD and in situ data for the three crop types with relevant important phenological stages.

Specifically, for Malagouzia in 2021, the cumulative SENSE-GDD values agree well with the in situ ones (Figure 5), but after May the differences between the two curves gradually increase to reach a cumulative discrepancy of −23.3°C on 31 July 2021. This corresponds to a relative difference of −1.7%. In 2022, the cumulative difference for Malagouzia at end date reaches −34.2°C, which corresponds to a relative difference of −2.4%. For Limnio, the differences are of similar magnitude and direction. Overall, at Epanomi, we observed (i) relative differences lower than 2.5% at the end of the season for

both years, (ii) slightly higher differences at the end of the period in 2022 than in 2021, and (iii) the early start of discrepancies between the two methods in 2022 than in 2021.

Concerning the Gran Smith apples (Figure 5), the difference between satellite-enabled and in situ GDD is negligible up to 25/05 but then starts to increase, reaching +110°C at the end of the studied period (27/07/2022). The relative difference between SENSE-GDD and the in situ data for the apple orchard at the end of the season is +9.5%.

In terms of the phenological stages, in 2021, the beginning of flowering and the start of veraison in the Malagouzia vineyard were observed on 21/05 and 18/07, respectively, while the corresponding dates in 2022 occurred just a few days earlier on 19/05 and 15/07 (Table 1). Limnio is found to develop slower than Malagouzia, as flowering and veraison started roughly 4–5 days later for both years. Using SENSE-GDD, the corresponding GDDs for flowering and pollination in 2021 are estimated to occur at the same dates with the in situ measurements while veraison is estimated to occur one day later (Table 1). For 2022, the budburst date is estimated to occur at the same date while the flowering and veraison are estimated to occur two days later for both grape types.

For the Gran Smith apples, the pollination estimated by SENSE-GDD seems to occur two days later than according to the in situ observations (Table 1). This practically means a two-day offset in the irrigation schedule.

Overall, the phenological stages that are associated with the observed GDDs are successfully calculated by SENSE-GDD for all three crop types, with a maximum offset of two days, making SENSE-GDD a reliable service for irrigation planning and other crop-related interventions that depend on GDDs.

3.4. Novelty and Limitations

SENSE-GDD overcomes two main issues related to the operational usage of temperature data derived from satellites. The first one is the presence of clouds in the TIR images that can result in missing data. To address this issue, a hybrid system is established [33] that seamlessly integrates satellite and weather prediction data into gapless AT datasets that allow the calculation of cumulative metrics, such as the GDD. The second issue is the coarse spatial resolution of geostationary satellites, for which an on-the-fly downscaling algorithm has been developed to enhance the spatial resolution of the AT image data. Due to their coarse resolution, geostationary data are rarely used in land applications, even though they offer an unparallel temporal resolution that enables the continuous monitoring of the surface of the Earth. SENSE-GDD employs a fast, lightweight, SVM-based downscaling algorithm that increases the spatial resolution of the AT data to 1 km, which allow for a more detailed analysis of environmental patterns and microclimatic variations. While finer-resolution data (e.g., 10 m) are preferred in agriculture applications, we consider the 1 km resolution adequate for monitoring the spatiotemporal variation of AT in rural areas and a major improvement compared to most numerical weather predictions and reanalysis data. The use of geostationary data, however, limits the use of SENSE-GDD to fields located only in Europe and Africa. This is because geostationary satellites are positioned at a specific point above the equator and can image an area that is typically limited to a specific hemisphere or a portion of it.

By definition, the accuracy of GDD retrieval is independent of the crop type. Different crops will only differ in base temperature. Therefore, the performance of the presented methodology depends on the assessment of AT which indeed can be different in different climatic conditions, but also depends on the time of the day, the season, and other dynamic factors. The performance of the AT retrieval has been exhaustively assessed in [33] in 15 selected areas in different climatic zones, where the main climatic factor is either Mediterranean Sea (Cairo, Athens, Barcelona, Cyprus, Istanbul, Lisbon, Mallorca, and Rome), Atlantic Ocean (Brussels, Hamburg, London, and Paris), or the continental part of Europe (Berlin, Madrid, and Zurich). Although the urban areas were the main focus of [33], other land cover types had also been included in the evaluation process (the land cover information was retrieved from the GlobCover). Specifically, 55 areas that were evaluated against station data corresponded to rural land cover type. The evaluation process also took into consideration the proximity to water as well

as the elevation. The evaluation considered hourly temperatures, a variable with higher variance than the daily average used in GDD, and demonstrated the good performance of the AT retrieval.

4. Conclusions

A new satellite-enabled interoperable service to provide high spatiotemporal and continuous time series of GDD data with a resolution of 1 km/1 h has been presented. The service covers designated agricultural pilot areas of the European project ATLAS. The capability of SENSE-GDD to derive reliable GDD time-series and to accurately predict key phenological stages is assessed using in situ air temperature measurements from weather stations installed in Epanomi (Northern Greece) and Agia (Central Greece) for the growing seasons of 2021 and 2022. Budburst, pollination and start of veraison are selected as key phenological stages for the wine grape vineyards at Epanomi; and budburst and the beginning of pollination for the apple orchard at Agia. The assessment shows that SENSE-GDD can provide reliable calculations of GDDs for all crop types with a maximum offset observed of two days. At the end of the season, the cumulative discrepancies in GDD were less than 2.5% for Epanomi (vineyards) and lower than 10% for Agia (apple orchard). The reader must acknowledge that point in situ measurements and satellite gridded values are, by definition, different. The question to answer with the performed evaluation is whether the satellite service can provide a trustworthy alternative to calculate GDDs in any non-instrumented field. With the presented evaluation and considering that the proposed service is fully automated and operational, we conclude that it can be especially valuable in non-instrumented crop fields, supporting decisions in a cost-effective way, and thus paving the way for its extended operational use in various agricultural applications.

Author Contributions: Conceptualization, I.K. and C.T.K.; methodology, I.K. and C.T.K.; software, I.K. and C.T.K.; validation, I.K., P.S., V.P., I.T., A.P., A.A. and C.T.K.; formal analysis, I.K., P.S., I.T. and C.T.K.; investigation, I.K. and C.T.K.; resources, I.K., A.P. and A.A.; data curation, I.K., I.T., P.S. and C.T.K.; writing—original draft preparation, I.K. and O.S.; writing—review and editing, I.K., P.S. and O.S.; visualization, P.S.; supervision, I.K.; project administration, I.K.; funding acquisition, I.K. All authors have read and agreed to the published version of the manuscript.

Funding: This project has received funding from the European Union's Horizon 2020 Research and Innovation Programme, under Grant Agreement No. 857125.

Data Availability Statement: All relative information regarding the work presented in this paper can be found in the official website of the ATLAS project: https://www.atlas-h2020.eu/. A detailed description of the system architecture, required authentication protocols during requests and analytical guidelines about how the services of each pool must implement their APIs can be found at https://github.com/atlasH2020-templates and https://github.com/atlasH2020 (both accessed on 23 April 2023).

Acknowledgments: The authors wish to thank Mallku Caballero from AgriCircle (Switzerland) for his collaboration to make the service interoperable in the ATLAS ecosystem and Stefan Rilling from Fraunhofer (Germany) for coordinating ATLAS project.

Conflicts of Interest: The authors declare no conflict of interest.

References

1. Ge, J.; Xu, Y.; Zhao, M.; Zhan, M.; Cao, C.; Chen, C.; Zhou, B. Effect of Climatic Conditions Caused by Seasons on Maize Yield, Kernel Filling and Weight in Central China. *Agronomy* **2022**, *12*, 1816. https://doi.org/10.3390/agronomy12081816.
2. Sacks, W.J.; Kucharik, C.J. Crop Management and Phenology Trends in the U.S. Corn Belt: Impacts on Yields, Evapotranspiration and Energy Balance. *Agric. For. Meteorol.* **2011**, *151*, 882–894. https://doi.org/10.1016/j.agrformet.2011.02.010.
3. Charalampopoulos, I.; Polychroni, I.; Psomiadis, E.; Nastos, P. Spatiotemporal Estimation of the Olive and Vine Cultivations' Growing Degree Days in the Balkans Region. *Atmosphere* **2021**, *12*, 148. https://doi.org/10.3390/atmos12020148.
4. Costa, R.; Fraga, H.; Fonseca, A.; de Cortázar-Atauri, I.G.; Val, M.C.; Carlos, C.; Reis, S.; Santos, J.A. Grapevine Phenology of Cv. Touriga Franca and Touriga Nacional in the Douro Wine Region: Modelling and Climate Change Projections. *Agronomy* **2019**, *9*, 210. https://doi.org/10.3390/agronomy9040210.
5. Kim, S.; Rho, H.Y.; Kim, S. The Effects of Climate Change on Heading Type Chinese Cabbage (Brassica Rapa L. Ssp. Pekinensis) Economic Production in South Korea. *Agronomy* **2022**, *12*, 3172. https://doi.org/10.3390/agronomy12123172.

6. Angel, J.R.; Widhalm, M.; Todey, D.; Massey, R.; Biehl, L. The U2U Corn Growing Degree Day Tool: Tracking Corn Growth across the US Corn Belt. *Clim. Risk Manag.* **2017**, *15*, 73–81. https://doi.org/10.1016/j.crm.2016.10.002.
7. Rodriguez, A.V.C.; Ober, E.S. AquaCropR: Crop Growth Model for R. *Agronomy* **2019**, *9*, 378. https://doi.org/10.3390/agronomy9070378.
8. Raes, D.; Steduto, P.; Hsiao, T.C.; Fereres, E. Aquacrop-The FAO Crop Model to Simulate Yield Response to Water: II. Main Algorithms and Software Description. *Agron. J.* **2009**, *101*, 438–447. https://doi.org/10.2134/agronj2008.0140s.
9. Jiang, X.; Liu, B.; Guan, X.; Wang, Z.; Wang, B.; Zhao, S.; Song, Y.; Zhao, Y.; Bi, J. Proper Deficit Irrigation Applied at Various Stages of Growth Can Maintain Yield and Improve the Comprehensive Fruit Quality and Economic Return of Table Grapes Grown in Greenhouses*. *Irrig. Drain.* **2021**, *70*, 1056–1072. https://doi.org/10.1002/ird.2624.
10. Tsakmakis, I.; Kokkos, N.; Pisinaras, V.; Papaevangelou, V.; Hatzigiannakis, E.; Arampatzis, G.; Gikas, G.D.; Linker, R.; Zoras, S.; Evagelopoulos, V.; et al. Operational Precise Irrigation for Cotton Cultivation through the Coupling of Meteorological and Crop Growth Models. *Water Resour. Manag.* **2017**, *31*, 563–580. https://doi.org/10.1007/s11269-016-1548-7.
11. Tursun, N.; Datta, A.; Sakinmaz, M.S.; Kantarci, Z.; Knezevic, S.Z.; Chauhan, B.S. The Critical Period for Weed Control in Three Corn (Zea Mays L.) Types. *Crop Prot.* **2016**, *90*, 59–65. https://doi.org/10.1016/j.cropro.2016.08.019.
12. Tepe, I.; Erman, M.; Yergin, R.; Bükün, B. Critical Period of Weed Control in Chickpea under Non-Irrigated Conditions. *Turk. J. Agric. For.* **2011**, *35*, 525–534. https://doi.org/10.3906/tar-1007-956.
13. Jamnani, M.R.; Mirzaei, F.; Liagat, A. Evaluation of sugarcane irrigation using AquaCrop model and remote sensing. *Irrig. Drain.* **2021**, *71*, 1034–1047. https://doi.org/10.1002/ird.2718.
14. Mwiya, R.M.; Zhang, Z.; Zheng, C.; Wang, C. Comparison of Approaches for Irrigation Scheduling Using AquaCrop and NSGA-III Models under Climate Uncertainty. *Sustainability* **2020**, *12*, 7694. https://doi.org/10.3390/su12187694.
15. Lalić, B.; Firanj Sremac, A.; Eitzinger, J.; Stričević, R.; Thaler, S.; Maksimović, I.; Daničić, M.; Perišić, D.; Dekić, L.J. Seasonal forecasting of green water components and crop yield of summer crops in Serbia and Austria. *J. Agric. Sci.* **2018**, *156*, 658–672. https://doi.org/10.1017/S0021859618000047.
16. Kassing, R.; De Schutter, B.; Abraham, E. Optimal Control for Precision Irrigation of a Large-Scale Plantation. *Water Resour. Res.* **2020**, *56*, e2019WR026989. https://doi.org/10.1029/2019WR026989.
17. Zaveri, E.; Lobell, D B. The role of irrigation in changing wheat yields and heat sensitivity in India. *Nat. Commun.* **2019**, *10*, 4144. https://doi.org/10.1038/s41467-019-12183-9.
18. Wang, K.; Su, L.; Wang, Q. Cotton Growth Model under Drip Irrigation with Film Mulching: A Case Study of Xinjiang, China. *Agron. J.* **2021**, *113*, 2417–2436. https://doi.org/10.1002/agj2.20667.
19. Djaman, K.; Irmak, S. Soil Water Extraction Patterns and Crop, Irrigation, and Evapotranspiration Water Use Efficiency of Maize under Full and Limited Irrigation and Rainfed Settings. *Trans. ASABE* **2012**, *55*, 1223–1238. https://doi.org/10.13031/2013.42262.
20. Irmak, S.; Odhiambo, L.O.; Specht, J.E.; Djaman, K. Hourly and Daily Single and Basal Evapotranspiration Crop Coefficients as a Function of Growing Degree Days, Days after Emergence, Leaf Area Index, Fractional Green Canopy Cover, and Plant Phenology for Soybean. *Trans. ASABE* **2013**, *56*, 1785–1803. https://doi.org/10.13031/trans.56.10219.
21. Tsakmakis, I.D.; Gikas, G.D.; Sylaios, G.K. Integration of Sentinel-Derived NDVI to Reduce Uncertainties in the Operational Field Monitoring of Maize. *Agric. Water Manag.* **2021**, *255*, 106998. https://doi.org/10.1016/j.agwat.2021.106998.
22. Zhu, P.; Burney, J. Untangling Irrigation Effects on Maize Water and Heat Stress Alleviation Using Satellite Data. *Hydrol. Earth Syst. Sci.* **2022**, *26*, 827–840. https://doi.org/10.5194/hess-26-827-2022.
23. Singh, G.; Das, N.N. A Data-Driven Approach Using the Remotely Sensed Soil Moisture Product to Identify Water-Demand in Agricultural Regions. *Sci. Total Environ.* **2022**, *837*, 155893. https://doi.org/10.1016/j.scitotenv.2022.155893.
24. Lekakis, E.; Zaikos, A.; Polychronidis, A.; Efthimiou, C.; Pourikas, I.; Mamouka, T. Evaluation of Different Modelling Techniques with Fusion of Satellite, Soil and Agro-Meteorological Data for the Assessment of Durum Wheat Yield under a Large Scale Application. *Agriculture* **2022**, *12*, 1635. https://doi.org/10.3390/agriculture12101635.
25. Thornton, M.M.; Shrestha, R.; Wei, P.E.; Thornton, P.E.; Kao, S.C.; Wilson, P.E.; Mayer, B.W.; Wei, Y.; Devarakonda, R.; Vose, R.S.; et al. *Daymet: Daily Surface Weather Data on a 1-km Grid for North America, Version 4 R1*; ORNL DAAC: Oak Ridge, TN, USA, 2020. https://doi.org/10.3334/ORNLDAAC/2129.
26. Climate Date Store (CDS) of Copernicus Climate Change Service. Available online: https://cds.climate.copernicus.eu/cdsapp#!/home (accessed on 12 April 2023).
27. Meng, J.; Mei, S.; Yan, Z. RESTful Web Services: A Solution for Distributed Data Integration. In Proceedings of the 2009 International Conference on Computational Intelligence and Software Engineering-CiSE 2009, Wuhan, China, 11–13 December 2009. https://doi.org/10.1109/CISE.2009.5365234.
28. Palma, F.; Olsson, T.; Wingkvist, A.; Gonzalez-Huerta, J. Assessing the Linguistic Quality of REST APIs for IoT Applications. *J. Syst. Softw.* **2022**, *191*, 111369. https://doi.org/10.1016/j.jss.2022.111369.
29. Kinikar, S.; Terdal, S. Implementation of Open Authentication Protocol for IoT Based Application. In Proceedings of the International Conference on Inventive Computation Technologies-ICICT 2016, Coimbatore, India, 26–27 August 2016. https://doi.org/10.1109/INVENTIVE.2016.7823267.
30. SEVIRI-Spinning Enhanced Visible InfraRed Imager. Available online: https://www.eumetsat.int/seviri (accessed on 12 April 2023).
31. Shuttle Radar Topography Mission. Available online: https://www2.jpl.nasa.gov/srtm/mission.htm (accessed on 12 April 2023).

32. NOAA Global Forecast System (GFS). Available online: https://www.nco.ncep.noaa.gov/pmb/products/gfs/ (accessed on 12 April 2023).
33. Keramitsoglou, I.; Kiranoudis, C.; Sismanidis, P.; Zakšek, K. An Online System for Nowcasting Satellite Derived Temperatures for Urban Areas. *Remote Sens.* **2006**, *8*, 306. https://doi.org/10.3390/rs8040306.
34. Sismanidis, P.; Keramitsoglou, I.; Bechtel, B.; Kiranoudis, C.T. Improving the Downscaling of Diurnal Land Surface Temperatures Using the Annual Cycle Parameters as Disaggregation Kernels. *Remote Sens.* **2017**, *9*, 23. https://doi.org/10.3390/rs9010023.
35. Sismanidis, P.; Keramitsoglou, I.; Kiranoudis, C.T.; Bechtel, B. Assessing the Capability of a Downscaled Urban Land Surface Temperature Time Series to Reproduce the Spatiotemporal Features of the Original Data. *Remote Sens.* **2016**, *8*, 274. https://doi.org/10.3390/rs8040274.
36. Sismanidis, P.; Keramitsoglou, I.; Kiranoudis, C.T. A Satellite-Based System for Continuous Monitoring of Surface Urban Heat Islands. *Urban Clim.* **2015**, *14*, 141–153. https://doi.org/10.1016/j.uclim.2015.06.001.
37. Sismanidis, P.; Keramitsoglou, I.; Kiranoudis, C.T. Evaluating the Operational Retrieval and Downscaling of Urban Land Surface Temperatures. *IEEE Geosc. Remote Sens. Lett.* **2015**, *12*, 1312–1316. https://doi.org/10.1109/LGRS.2015.2397450.
38. McMaster, G.S.; Wilhelm, W.W. Growing Degree-Days: One Equation, Two Interpretations. *Agric. For. Meteorol.* **1997**, *87*, 291–300. https://doi.org/10.1016/S0168-1923(97)00027-0.
39. Steduto, P.; Hsiao, T.C.; Raes, D.; Fereres, E. Aquacrop-the FAO Crop Model to Simulate Yield Response to Water: I. Concepts and Underlying Principles. *Agron. J.* **2009**, *101*, 426–437. https://doi.org/10.2134/agronj2008.0139s.
40. Savé, R.; de Herralde, F.; Aranda, X.; Pla, E.; Pascual, D.; Funes, I.; Biel, C. Potential Changes in Irrigation Requirements and Phenology of Maize, Apple Trees and Alfalfa under Global Change Conditions in Fluvià Watershed during XXIst Century: Results from a Modeling Approximation to Watershed-Level Water Balance. *Agric. Water Manag.* **2012**, *114*, 78–87. https://doi.org/10.1016/j.agwat.2012.07.006.